

Spectroscopic Pulsational Frequency Identification and Mode Determination of γ Doradus Star HD 12901 ^{*}

E. Brunsden^{1†}, K. R. Pollard¹, P. L. Cottrell¹, D. J. Wright², P. De Cat³

¹*Department of Physics and Astronomy, University of Canterbury, Private Bag 4800, Christchurch, New Zealand*

²*Department of Astrophysics, University of New South Wales, Sydney, NSW 2052 Australia*

³*Royal Observatory of Belgium, Ringlaan 3, 1180 Brussel, Belgium*

September 28, 2012

ABSTRACT

Using multi-site spectroscopic data collected from three sites, the frequencies and pulsational modes of the γ Doradus star HD 12901 were identified. A total of six frequencies in the range 1–2 d^{−1} were observed, their identifications supported by multiple line-profile measurement techniques and previously-published photometry. Five frequencies were of sufficient signal-to-noise for mode identification and all five displayed similar three-bump standard deviation profiles which were fitted well with $(l, m) = (1, 1)$ modes. These fits had reduced χ^2 values of less than 18. We propose that this star is an excellent candidate to test models of non-radially pulsating γ Doradus stars as a result of the presence of multiple $(1, 1)$ modes.

Key words: line: profiles, techniques: spectroscopic, HD12901, stars: variables: general, stars: oscillations

1 INTRODUCTION

The identification of the geometry of a γ Doradus type pulsation remains one of the more difficult spectroscopic fields. However, it is a powerful way to characterise the interior structure of a star and improve stellar pulsation models. The pulsations of γ Doradus stars are particularly of interest as they propagate through the deep layers of a star. The flux-blocking mechanism at the base of the surface convective zone (Guzik et al. 2000) is held accountable for the origin of the pulsations which are g-modes, where the restoring force is gravity.

Briefly γ Doradus stars are slightly evolved late-A to late-F stars at the cooler end of the classical instability strip that display high-order g-mode pulsations with frequencies on the order of 1 cycle-per-day. For a full definition see Kaye et al. (1999) and recent reviews of the field are in Kaye (2007) and Pollard (2009). Currently there are less than 100 bright bona fide γ Doradus stars known (see list in Henry et al. 2011) and a handful of γ Doradus/ δ Scuti hybrid stars (Henry & Fekel 2005; Uytterhoeven et al. 2008), with a further 100 γ Doradus and 171 hybrid stars thus far reported

by the *Kepler* mission (Grigahcène et al. 2010; Uytterhoeven et al. 2011).

Now is truly the age of satellite photometry and no ground-based methods can compete with the long uninterrupted datasets that satellites such as *CoRoT* and *Kepler* produce. The Fourier frequency spectra of such studies show the high-levels of precision only obtainable from space (e.g. at least 840 frequencies found in HD 49434 using the *CoRoT* satellite; Chapellier et al. 2011). However, to further our understanding of g-mode pulsations we need more data than frequencies alone. Several successful techniques using ground-based multi-colour photometry can be employed to determine the number of nodal lines (l) in a star. The full mode-identification of a star, that is finding the l and also the number of nodal lines passing through the pole of a star m , remains the sole domain of spectroscopy. It is hoped that modelling of the frequencies and modes of a star will allow determination of the n , number of shells interior to the stellar surface.

The spectroscopic study of γ Doradus stars relies on the collection of a large amount of high-resolution and preferably multi-site data of sufficient signal-to-noise for classification of the pulsations. Improvement is gained by the use of data from multiple sites to reduce daily aliasing patterns in the Fourier spectra. Such observational campaigns take many months to years in order to collect a sufficient number of spectra.

When such datasets are compiled for γ Doradus stars, the pulsational frequencies and modes can be examined and

^{*} This paper includes data taken at the Mount John University Observatory of the University of Canterbury (New Zealand), the McDonald Observatory of the University of Texas at Austin (Texas, USA), and the European Southern Observatory at La Silla (Chile).
[†] E-mail: emily.brunsdens@gmail.com

Table 1. Observation log of the multi-site data for HD 12901

Observatory	Telescope	Spectrograph	Observation range	ΔT (d)	# spectra
MJUO	1.0m	HERCULES	Feb 2009-Sep 2011	935	478
La Silla	1.2m	CORALIE	Nov 1998-Nov 2002	1166	53
McDonald	2.1m	SES	Sep 2009-Oct 2009	8	60

compared to those from photometry. There are still only a handful of γ Doradus stars with full mode identifications and our immediate goal is to classify as many as we can. The results of these mode identifications can be used to improve pulsational models (such as those of Grigahcène et al. 2012; Townsend 2003) by providing information about the amplitudes of excited modes and also to start to identify patterns within the class.

This paper focuses on the γ Doradus star HD 12901 outlining the observations made and reduction procedure in Section 2. The spectroscopic frequency analysis for the individual observatories and the combined data results are described in Section 3 with each method tested. Section 4 describes the reanalysis of white-light and seven-colour photometry taken of this star. The mode identification of the five identified frequencies follows in Section 5. Finally Section 6 discusses the findings and their implications for future work in this field.

2 OBSERVATIONS AND DATA TREATMENT

The major findings of this research are the identification of the frequencies and modes using spectra obtained at three observing sites (Mt John University Observatory (MJUO), La Silla Observatory and McDonald Observatory) and are summarised in Table 1.

Spectra were reduced according to the standard local spectrograph software then they were normalised, continuum fitted and order-merged by the authors using a semi-automated MATLAB routine. The full spectra were cross-correlated for each site using a scaled delta function routine (Wright 2008, Wright et al. 2007). This produces the line profiles used for pulsational analysis. The signal-to-noise of a cross-correlated line profile is much higher than a single spectral line and thus pulsations are easier to extract. The line profiles for each site were combined (scaled, shifted in velocity space and continuum fitted) to produce a single dataset of consistent line profiles. This was done post-cross correlation to maximise the number of available lines used for each spectrum, as different spectrographs operate over different wavelength ranges.

The line profiles were analysed in FAMIAS, a pulsational frequency mode-identification toolbox (Zima 2008), using techniques applied from Zima et al. (2006). The Fourier spectra for the Pixel-by-Pixel (PbP) technique and that of the 0th-3rd moments (Balona 1986; Briquet & Aerts 2003) were used to identify frequencies. These frequencies were then analysed to determine mode identifications using the Fourier Parameter Fit method (Zima 2009).

Additionally, the software package SIGSPEC (Reegen 2007) was used to compare the frequency selection method of FAMIAS. SIGSPEC performs a Fourier analysis of a two-dimensional dataset and selects frequencies based on their spectral significance. The frequencies obtained with SIGSPEC

can be regarded as more precise than that of the highest-peak direct selection as, after producing the Fourier frequency spectrum, the peak with the highest spectral significance is selected. Spectral significance includes the analysis of the false-alarm probability to remove frequency peaks caused by irregular data sampling or noise in the data.

Both FAMIAS and SIGSPEC were used to re-analyse photometric data, originally published in Handler (1999), Eyer & Aerts (2000) and Aerts et al. (2004), as further insight into the frequencies of the pulsations. To identify the l values of the modes, the frequency amplitude ratio and phase differences method, based on pre-computed grids of models, were used (Balona & Stobie 1979; Watson 1988; Cugier et al. 1994; Daszyńska-Daszkiewicz et al. 2002). This was done using the photometric analysis toolbox in FAMIAS (Zima 2008).

3 SPECTROSCOPIC FREQUENCY ANALYSIS

In total 591 spectra from the three sites were of sufficient quality to be analysed. The data spanned a total of 4667 days, just over 12 years. Each dataset was analysed independently for frequencies and they were then combined. By doing this analysis we can comment on the limitations of single-site data and the extent to which multi-site data reduces aliasing.

3.1 Frequency Identification For Each Dataset

3.1.1 MJUO

This is the largest single-site dataset and was analysed most extensively. First the cross-correlated line profiles were analysed in FAMIAS. The frequency list is in Table 2. The PbP technique found eight possible frequency peaks including a one-cycle-per-day frequency (f_{m5}), likely an alias. The zeroth moment was too noisy to extract any frequencies. The first and third moment Fourier peaks each only showed one frequency clearly, 1.186 d^{-1} and 1.184 d^{-1} respectively, which is the same frequency given a conservative uncertainty estimate of ± 0.001 (uncertainties are dealt with more formally in Section 3.3). The second moment yielded 0.144 d^{-1} as the only viable frequency. Though many more frequencies may be evident in the data, further extraction of frequencies above the noise was difficult with any measure of certainty.

The same moments were then tested in SIGSPEC for further analysis. SIGSPEC found 20 frequencies above a spectral significance level of 5. It is likely that noise in the data is causing many misidentifications rather than the possibility that these could all be real, given the noise level in the Fourier spectra. The frequencies with spectral significance greater than 15 are reported for moments one to three in Table 2. From the table it is clear that f_{m2} to f_{m8} (excluding f_{m5}) are viable frequencies found using multiple methods. The addition of further datasets from other observation sites

should improve the signal-to-noise and reduce any aliasing, particularly 1-day aliasing that occurs in the data.

3.1.2 La Silla

The spectra taken on the CORALIE spectrograph have previously been analysed and published by Aerts et al. (2004) and De Cat et al. (2006). Frequencies of $1.04 \pm 0.28 \text{ d}^{-1}$ and $1.30 \pm 0.30 \text{ d}^{-1}$ were reported.

Although the small size of the dataset made it difficult to analyse, frequency peaks were identified at 0.005 d^{-1} and 1.26 d^{-1} in the PbP measure, 0.997 d^{-1} and 3.01 d^{-1} in the first moment and 0.997 d^{-1} and 1.999 d^{-1} in the third moment. Peaks that occur very close to integer values are less reliable as they are likely 1-day alias patterns from the observation times artificially amplified by data sampling effects in the window function. No identifiable peaks occurred in the zeroth and second moments. Only the 1.26 d^{-1} can be identified with any confidence. It is notable that a peak was apparent in all the above Fourier spectra at 0.23 d^{-1} .

SIGSPEC was better able to distinguish the 1-day aliases and identified frequencies of 0.26 d^{-1} in the zeroth moment and 0.23 d^{-1} in the first and third moments. These had significances of 3.3, 3.5 and 2.7 respectively, which are usually regarded as too small to be significant.

3.1.3 McDonald

The McDonald data set comprised of 60 observations taken in September and October 2009. The data were considered to be particularly useful as having time intervals that overlap some of the MJUO observations, providing some independent confirmation of the line profile variation. As a stand-alone data set the shorter wavelength range of the spectrograph, and the larger regions of telluric lines, reduced the number of stellar lines that could be cross-correlated from several thousand to around 100 lines. This has a significant impact on the signal-to-noise of the final line profile. This, and the low number of observations, meant frequencies detected in this dataset alone were unconvincing. Despite this, it is noted that frequencies near 1.38 d^{-1} and 1.24 d^{-1} are present in the PbP analysis and a peak near 1.67 d^{-1} is visible in the first moment Fourier spectrum.

3.2 Frequency Identification Of Combined Data For Each Method

The cross-correlated line profiles of the three datasets were combined post cross-correlation to form a single dataset. The line profiles are displayed in Figure 1. Combining the line profiles instead of the individual spectra was the best way to preserve the signal-to-noise in the MJUO and La Silla datasets which had many more lines than the McDonald spectra. There was a small shift (6 km s^{-1}) in the systemic velocity between the McDonald and the other two datasets. The McDonald spectra were shifted to ensure consistent data. The line profiles were scaled to have the same equivalent widths, a parameter shown to remain constant by the lack of variation in the zeroth moment in the MJUO data. The Fourier spectra of the MJUO data alone and the combined datasets are compared in Figure 2.

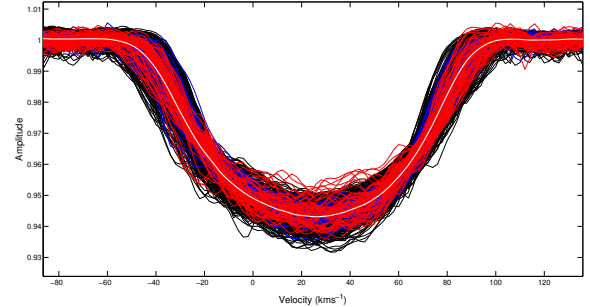


Figure 1. Scaled line profiles of the three datasets. McDonald (red), La Silla (blue) and MJUO (black) observations are shown with the mean line profile (white). All datasets scale well to show a consistent line profile. The data are provided as an electronic file (see Supporting Information).

The spectral windows for the MJUO data alone and all three data sets are very similar, but, as expected, the addition of the multi-site data reduces the amplitude of the secondary peaks of the identified frequency. From Figure 2 it is clear that the addition of the extra data increases the amplitude of the Fourier peaks. This is an effect of not only the reinforced signal found in the other sites spectra, but also an artificial amplification due to the increased base noise level. The frequency peaks remain in nearly the same positions and show approximately the same repeating pattern. The one-day aliasing, although still present, has been reduced to make the true peaks more evident. In general, the frequency identification becomes clearer with the addition of the multi-site data, despite it being from small sets compared to the MJUO data.

3.2.1 Pixel-by-Pixel (PbP)

The line profiles showed many periodic variations in each pixel. The ten frequencies found in the combined dataset are listed in Table 3 and the Fourier spectra displayed in Figure 2. The first two frequencies found were the f_2 and f_3 from Aerts et al. (2004) from photometry and their f_1 shows up as our f_{p4} . Further frequencies f_{p3} and f_{p5} have credible three bump variations in their line profiles. It is likely that f_{p6} is a one-day alias frequency arising from the dominance of one single site (MJUO contributes about 80% of the observations). The frequencies f_{p7} , f_{p8} and f_{p10} showed clear three bump standard deviation profiles each with smooth phase changes. This increases the likelihood that they are real frequencies, although the possibility remains that they are from residual power from a previous poorly-defined frequency. Finally, f_{p9} showed a clear four bump standard deviation profile at 3.14 d^{-1} and 4.14 d^{-1} frequencies when tested. As none of the previous frequencies showed a four-bump pattern in the variation it is more likely this is a real frequency rather than a misidentification of an earlier frequency.

A check on the independence of the frequencies was done by prewhitening the spectra by 1-day aliases and 1- f aliases of the first five identified frequencies. Only $f_{p3} \pm 1$ had clear standard deviation profile variations resembling pulsation and none of the alternate identifications altered

Table 2. Frequencies of HD 12901 found in the MJUO data. Pixel-by-Pixel (PbP) frequencies found using FAMIAS and moments and significances (Sig) found using SIGSPEC are listed. The amplitudes of the PbP frequencies are scaled to the first identified amplitude. Note some frequencies have been identified as $1 - f$ aliases of the PbP frequency. The frequency f_{m5} shows identifications near 1 d^{-1} , likely from the data sampling.

	PbP			Moments				
	Freq. (d ⁻¹)	Amp. (rel. to <i>f_{m1}</i>)	1 st (d ⁻¹)	Sig	2 nd (d ⁻¹)	Sig	3 rd (d ⁻¹)	Sig
<i>f_{m1}</i>	1.271	1						
<i>f_{m2}</i>	1.186	1.8	1.183	24			1.183	23
<i>f_{m3}</i>	1.681	1.5	0.678	26			0.678	28
<i>f_{m4}</i>	1.396	1.7	0.403	20	1.396	20		
<i>f_{m5}</i>	1.001	1.3			1.001	26		
<i>f_{m6}</i>	1.560	1.6	0.460	16	1.560	17	1.560	19
							0.541	18
<i>f_{m7}</i>	1.216	1.6	2.214	18	0.213	23	2.214	20
<i>f_{m8}</i>	0.244	1.1	0.756	21				
<i>f_{m9}</i>					0.104	16	0.899	19
<i>f_{m10}</i>							2.352	20
<i>f_{m11}</i>							0.836	17

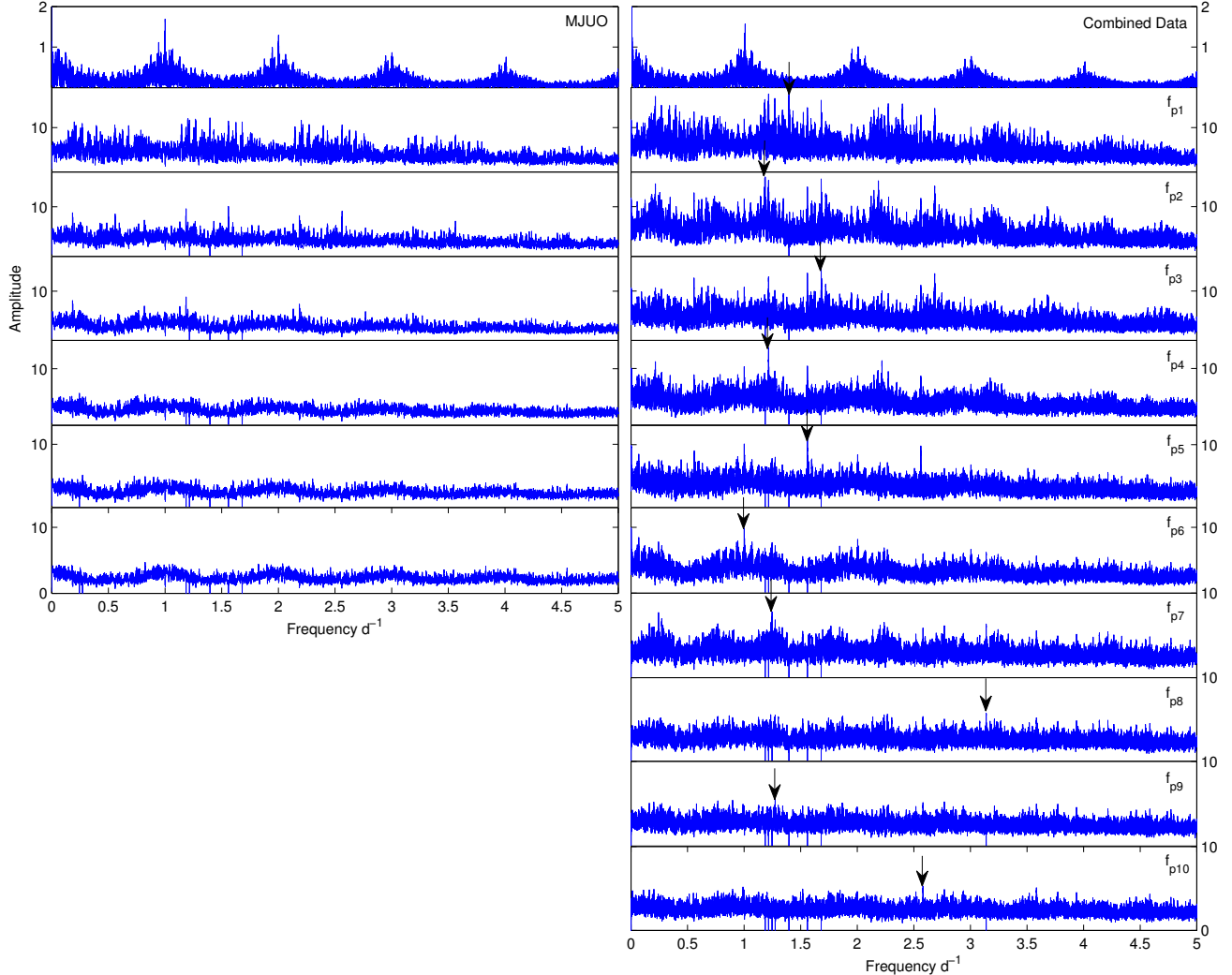


Figure 2. Effect of the multi-site datasets on the Pixel-by-Pixel Fourier spectra, the MJUO data on the left and the combined data on the right. Each series shows the window function for the data at the top then successive pre-whitening of frequencies f_{p1} to f_{p5} . The Fourier spectra for the Pixel-by-Pixel analysis of the combined data continues to f_{p10} . The frequencies are listed in Table 3.

Table 3. Frequencies from the Pixel-by-Pixel analysis of the combined dataset. The uncertainty estimate for the frequencies is $\pm 0.0002 \text{ d}^{-1}$ as described in Section 3.3. Frequencies with a strike-through were discarded as described in the text.

ID	Freq. (d^{-1})	Period (d)	Amp. (rel. to f_{p1})	Phase	Variation Explained
f_{p1}	1.3959	0.7164	1	0.286	13%
f_{p2}	1.1863	0.8430	0.72	0.205	21%
f_{p3}	1.6812	0.5948	0.93	0.267	30%
f_{p4}	1.2157	0.8226	0.93	0.265	39%
f_{p5}	1.5596	0.6412	0.80	0.230	45%
f_{p6}	1.0004	0.9996	0.55	0.158	48%
f_{p7}	1.2465	0.8022	0.50	0.143	50%
f_{p8}	1.2743	0.7848	0.53	0.152	53%
f_{p9}	3.1392	0.3186	0.36	0.102	54%
f_{p10}	2.5803	0.3876	0.37	0.106	55%

the identification of following frequencies, indicating that they are all independent.

A second check of the variability of the line profile with different frequencies involves phasing the data to the proposed frequency and examining the structure. To see the changes most clearly this was done using the residuals of the line profiles after subtraction of the mean. The frequencies f_{p1} to f_{p5} in Figure 3 the residuals on the left side of each plot show the ‘braided rope’ structure typical of non-radial pulsation, but for the other frequencies this was less clear. If we require pulsations to produce regular changes in both red and blue halves of the line profile then we must discard f_{p6} , f_{p7} and f_{p9} as candidate frequencies leaving just f_{p8} and f_{p10} to investigate further.

An investigation into the phase coverage of the data for each frequency can also be used as an indicator of the reliability of the frequency. All of the frequencies $f_{p1} - f_{p10}$ were well covered in phase space except f_{p6} , which was poorly sampled between phases 0.2-0.3 and 0.5-0.8 due to the dominance of a single site in the data.

3.2.2 Moment Analysis

The zeroth moment analysis shows few peaks that are similar to those from other methods. There is a cyclic variation around 1-cycle per day but with the 1.0 d^{-1} peak missing due to the combination of multi-site data. The small amplitude of variations in the second moment indicates we have only small periodic temperature variations to account for in the line profiles.

The first moment Fourier spectra showed clear peak frequencies similar to the PbP method. These are shown in the first section of Table 4. The amount of variation of the first moment was moderately well explained by the selection of the highest six peaks in the Fourier spectrum. Beyond f_{f6} the improvements to the explanation of variation are too small to be conclusive. When the PbP frequencies were extracted from the first moment data (in approximately the same order as the highest peak frequencies) a better fit to the variation was found. With the six frequencies, $f_{p1} - f_{p5}$ and f_{p8} , 76% of the variation was removed. The frequencies found using SIGSPEC closely matched the first four frequen-

cies found in the highest peak method then reproduced PbP frequencies f_{p3} and f_{p7} as f_{f9} and f_{f10} .

The Fourier spectra of the second moment also showed a few promising frequencies once the first peak at 0.0006 d^{-1} was removed. The frequencies f_{s2} to f_{s4} match to, or match to one-day aliases of, frequencies found in the PbP dataset. It is likely that f_{s6} is a misidentification of f_{p2} . The second section of Table 4 catalogues the frequencies found. Both the highest peak and PbP frequencies accounted for around the same amount of variation as they identified nearly all the same frequencies.

Frequency peaks found in the third moment are presented in the final section of Table 4. The first few frequencies found using this method were generally similar to those found in the PbP method except the double identification of f_{t2} . This is usually the result of small errors in the identification of a strong frequency, leaving residual power in the Fourier spectrum. It is likely that this then impacts the following sequence f_{t5} to f_{t10} which all seem close frequencies to other identifications, and possibly one-day aliases. The PbP frequencies identified explained more variation, accounting for a total of 83% of the line profile variation.

Overall the PbP variations have been shown to remove the variation from the data more accurately, demonstrated by the higher percentage of variation removed for each moment. This leads us to conclude that the frequencies found using the highest peaks in the moment methods are less reliable. It is notable that the SIGSPEC identified frequencies are more reliable than the highest peak selection.

As an additional test of the robustness of the derived frequencies, a synthetic dataset, modelled on the time spacings and modes identified in Section 5, was created to compare with the PbP derived frequencies. The synthetic line profiles were phased and plotted to compare with the real data in Figure 3. The synthetic profiles strongly match the observed profiles, strengthening our confidence in the frequency identification.

3.3 Frequency Results

The frequencies chosen to proceed with in the analysis were those originally identified in the PbP results, f_{p1} to f_{p5} and f_{p8} as noted in Table 3. This choice was made based on the prevalence of these frequencies through the other techniques used, the decreased sensitivity of the PbP technique to asymmetric variations and generally observed higher signal-to-noise of the PbP frequencies.

It is clear from the above sections that, due to the inclusion of multi-site data, 1-day aliasing was not a big problem when identifying frequencies present in these data.

Identifying the uncertainty range on the frequencies found is a complex task. When using SIGSPEC we can use the relation of Kallinger et al. (2008):

$$\sigma(f) = \frac{1}{T * \sqrt{\text{sig}(a)}}, \quad (1)$$

where T is the time base of observations in days and $\text{sig}(a)$ is the spectral significance of the frequency. For the frequencies f_{p1} to f_{p10} identified in the first moment method this gives an uncertainty estimate of ± 0.0002 . Additionally we used

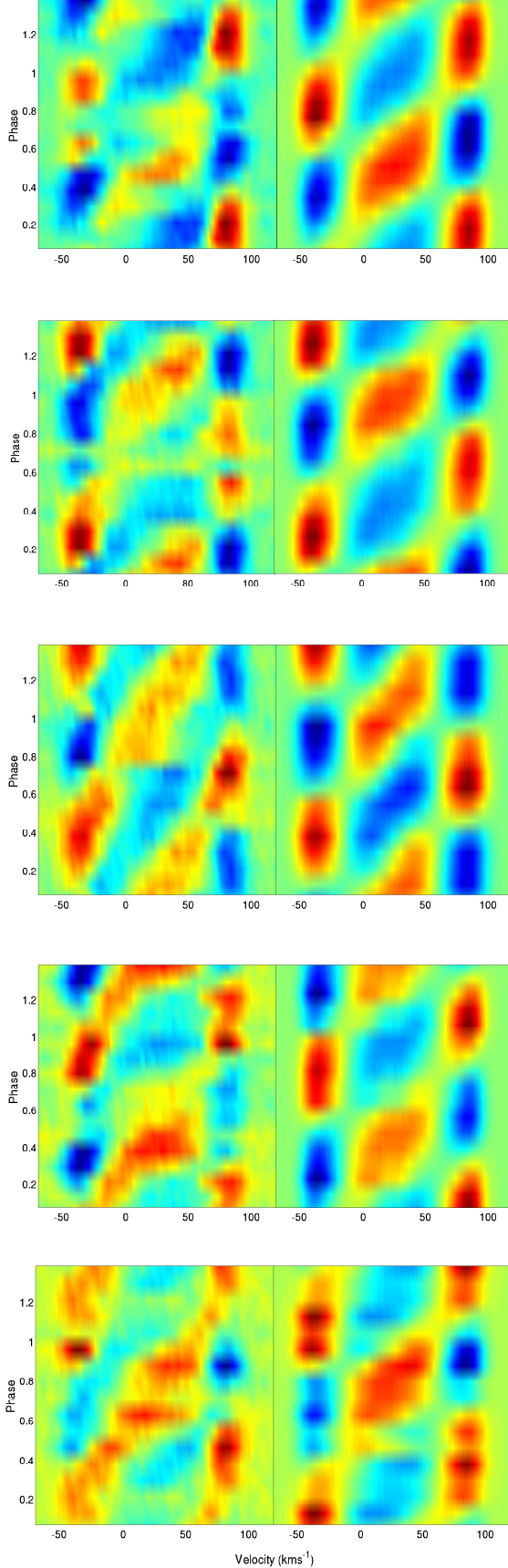


Figure 3. Line profile residuals phased on the frequencies identified f_{p1} (top) to f_{p5} (bottom) compared with synthetic profiles. The left panel shows the observed profiles and the right is

Table 4. Resulting frequencies from the First, Second and Third Moments found using peaks in the Fourier spectra and in SIGSPEC

First Moment

ID	Highest Peak		SIGSPEC	
	Freq.	Var.	Freq.	Sig.
f_{f1}	1.1835	16%	1.18624	26
f_{f2}	1.6100	32%		
f_{f3}	1.4017	42%	1.39591	26
f_{f4}	1.2247	52%	1.2156	28
	1.2154		2.2273	21
f_{f5}	0.6490	57%		22
f_{f6}	1.5627	63%	1.5596	20
f_{f7}	0.7559	66%		
f_{f8}	1.5179	69%		
f_{f9}			1.6812	22
f_{f10}			0.2436	22
f_{f11}			2.1362	17
f_{f12}			0.0002	17
f_{f13}			2.7789	15
f_{f14}			0.6736	15

Second Moment

ID	Highest Peak		SIGSPEC	
	Freq.	Var.	Freq.	Sig.
f_{s1}	0.0006	7%		
f_{s2}	0.2159	22%		
f_{s3}	0.3767	38%		
	1.3962		1.3959	19
f_{s4}	1.5596	46%	1.5596	20
f_{s6}	2.1786	57%		
f_{s7}			0.1622	25
f_{s8}			0.9449	23
f_{s9}			0.9061	19
f_{s10}			0.7382	19
f_{s11}			2.6809	17

Third Moment

ID	Highest Peak		SIGSPEC	
	Freq.	Var.	Freq.	Sig.
f_{t1}	1.3987	17%	1.3956	31
f_{t2}	1.1864	40%	1.1862	25
	2.1833			
f_{t3}	1.6810	49%	1.6809	23
f_{t4}	1.3489	58%		
f_{t5}	1.1661	64%		
f_{t6}	2.5624	32%	0.5597	21
f_{t7}	2.7952	41%		
f_{t8}	1.1716	49%		
f_{t9}	3.5169	58%		
f_{t10}	1.2658	64%		
f_{t11}			1.2156	27
f_{t12}			2.1923	20
f_{t13}			0.2437	18

the estimation from Montgomery & Odonoghue (1999) who propose

$$\sigma(f) = \sqrt{\frac{6}{N}} \frac{1}{\pi T} \frac{\sigma(m)}{A}. \quad (2)$$

Here N is the number of observations. The value $\sigma(f)$ is

Table 5. Frequencies found in the HIPPARCOS white-light photometry. The first three frequencies match well with f_{p4} , f_{p5} and f_{p7} .

Frequency (d^{-1})	Uncertainty	Significance
1.2158	± 0.0003	7
1.5525	± 0.0003	6
2.2449	± 0.0003	6
2.5665	± 0.0004	5

a one-sigma uncertainty with an amplitude (A) root-mean-square deviation $\sigma(m)$. This method was used to derive (an underestimate) of the uncertainties of the pixel-by-pixel frequencies. The results for the frequencies f_{p1} to f_{p5} ranged from ± 0.00013 to ± 0.00018 . Given the observed differences between the frequencies identified in the PbP and the moment methods we view ± 0.0002 to be a good estimate of the uncertainty.

The data were also analysed for possible frequency combinations. It was found that $f_{p5}(1.559) + f_{p3}(1.681) = 3.240\text{d}^{-1}$ which is possibly the same as $f_{p7}(1.246)$ and strengthens our earlier removal of this frequency.

It is clear from the above sections that many frequencies extracted from the data are robust as they appear in multiple methods with clear line profile variations. The first five frequencies in the PbP analysis appear in almost every analysis method. The high signal-to-noise in the line profiles for these frequencies makes them suitable for mode identification. The frequency f_{p8} , although showing evidence for being an independent frequency, showed a misshapen standard deviation profile, which meant there was not enough certainty in this frequency identification to proceed with a mode identification. The final PbP frequency f_{p10} showed no evidence of appearing in other analysis methods and was rejected for mode identification.

Even with all these frequencies identified, variations in the data remain. The PbP method only removed 50% of the variation and the moment methods up to 80%. Some of the remaining variation is due to the noise in the data and possible slight misidentifications of the frequencies, but it is likely that there remain multiple unidentified frequencies below the detection threshold of the present data. The presence of these further frequencies is expected for γ Doradus stars as they have dozens and sometimes even hundreds of frequencies identifiable in photometry. The large number of similar amplitude frequencies make this star challenging to study. However already we are able to see more frequencies than previously identified in spectroscopy, which makes this a promising star for further study.

4 PHOTOMETRIC FREQUENCY AND MODE IDENTIFICATION

Two photometric datasets were analysed for frequencies. The first was a time series of white light observations from the satellite HIPPARCOS (Perryman & ESA 1997). Specifically these were taken in the H_p filter. The data span a period of 1166 days from November 1989 to February 1993 during which 122 measurements were taken. The second dataset was Geneva photometry taken on the 0.7m Swiss telescope

at La Silla over a period of 25 years from 1973 to 1997. A total of 174 observations for each filter in this time. This dataset has been extensively analysed in Aerts et al. (2004). We present our re-analysis to complement the spectroscopic results above.

4.1 HIPPARCOS Photometric Frequencies

The Fourier analysis of the HIPPARCOS data measurements have a range of 0.09 H_p magnitudes with an average uncertainty of 0.1 H_p magnitudes. It was difficult to identify clear frequencies from the Fourier spectra, but the highest peak was at 1.2701d^{-1} . Using SIGSPEC we were able to identify the frequencies and their significances as shown in Table 5.

4.2 Geneva Photometric Frequencies

The seven filters of the Geneva photometry provide us with enough information to extract frequencies and identify the l modes. Each of the seven filters showed very similar variation and this was reflected in the individual Fourier spectra. Frequency peaks were observed at 1.218d^{-1} , 1.396d^{-1} and 0.0907d^{-1} (or one-day aliases) in most filters. To formalise the frequency identification we used SIGSPEC to identify the frequencies and their significances as shown in Table 6. These frequencies match well to those previously found in the same data as is discussed further in Section 6.

4.3 Geneva Photometry Modes

The identification of the l value of the spectroscopic frequencies f_{p1} to f_{p5} was attempted using the seven filters in the Geneva photometric data. The identification was done using the amplitude ratio method in FAMIAS with modes from $l = 1$ to $l = 3$ tested in all filters. All five frequencies were found to be solely consistent with $l = 1$ modes distinguished primarily by the first amplitude ratio. The results are largely identical to Aerts et al. (2004), Their Figure 6 shows the unique fit to the $l = 1$ mode. This method, although not as powerful as spectroscopic mode identification, gives us independent support to the $l = 1$ mode fits of the star.

5 MODE IDENTIFICATION OF SPECTROSCOPIC LINE PROFILES

The mode identification was performed using the PbP frequencies f_{p1} to f_{p5} , as chosen in Section 3.3 (f_{p8} not being considered due to the distorted line profile variations). The modes of the individual frequencies were first identified and then a best fit, including all five frequencies, was computed. Initially the zero-point profile was fitted to determine the basic line parameters. The best fit is shown in Figure 5(a). The $v\sin i$ was found to converge at 63.9km s^{-1} with a χ^2 of 103. Figure 4 shows the 95% confidence limit on the determination of $v\sin i$ which gives a range of $63.9 \pm 0.5\text{km s}^{-1}$. The zero-point fit set the initial line and stellar parameters of the space searched. The details of the parameters are given in Table 8 and the resulting best fit modes are given in Table 9.

Table 6. Frequencies (d^{-1}) found in each of the Geneva photometry filters and significances using SIGSPEC.

	B		B1		B2		G		U		V		V1	
	f.	sig.	f.	sig.	f.	sig.	f.	sig.	f.	sig.	f.	sig.	f.	sig.
f_1	1.215	13	1.215	13	1.215	12	2.218	11	1.215	13	1.215	11	1.215	12
f_2	0.09	8	0.09	8	0.09	8	0.393	6	0.07	5	0.09	7	0.095	8
f_3	1.396	8	1.396	8	1.396	8	0.071	6			1.396	7	1.396	6
f_4	2.567	5	1.565	5	3.56	4	3.32	5			4.32	4	3.32	6
f_5							3.19	4					2.95	4

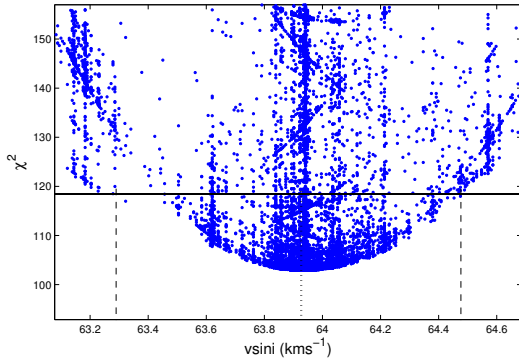


Figure 4. The 95% confidence limit (solid line) of the zero-point fit to the $vsini$. The dashed lines show the limits at the confidence level and the dotted line indicates the minimum and hence best fit value.

The unusually high values for mass and radius are discussed in Section 5.1.

The best fit models for each individual frequency are plotted in Figures 5(b) - 5(f). The results in Table 9 and Figures 6(a) to 6(e) show that the mode identifications are well determined as there is no ambiguity in choosing the model with the lowest χ^2 . The inclination appears to lie in the region $20^\circ - 45^\circ$, with the simultaneous fit giving a value of 27° for a χ^2 of 16.59. Formally the 95% confidence limit of this parameter gives $27^\circ {}^{+52}_{-12}$, so it is poorly constrained by the mode identification. Given the $vsini$ of the star, a value near 30° is plausible as described further in Section 5.1. The $vsini$ value determined varies slightly between the fits as it is modified to change the width of the standard deviation profile. The measured $vsini$ of the star is best determined from the fit to the zero-point profile given above.

The detection of five independent frequencies and the occurrence of a large number of (1,1) modes makes this star an excellent candidate for further asteroseismic analysis. The prevalence of the (1,1) modes may indicate sequencing of the n -values, or the number of interior shells. It also is possible that the (1,1) modes may be linked to the rapid rotation of the star. This is discussed in the context of all γ Doradus stars in Section 6.

5.1 Rotation and Pulsation Parameters

The results of a preliminary mode identification were tested using the rotation and pulsation parameter tools in FAMIAS. Using mass = $1.5 M_\odot$ and radius = $1.7 R_\odot$ (typical for a γ Doradus star), $vsini = 64 \text{ km s}^{-1}$ and various inclinations indicates the rotational parameters of the star. Shown in Table 7 are the results for $i = 30^\circ$, which indicates that this

Table 7. Rotational parameters and critical limits for a pulsating star with mass = $1.5 M_\odot$, radius = $1.7 R_\odot$, $vsini = 64 \text{ km s}^{-1}$ observed at an inclination of $i = 30^\circ$.

v_{rot}	128 km s^{-1}
T_{rot}	0.67 d
f_{rot}	1.49 d^{-1}
v_{crit}	410 km s^{-1}
$vsini_{crit}$	205 km s^{-1}
i_{crit}	9°

star is not approaching critical rotational velocity. This is the case for all tested values of i in the range $i = 10^\circ - 90^\circ$. The rotational frequency of the star is dependent on the inclination, ranging from 4.28 d^{-1} at $i = 10^\circ$ to 0.74 d^{-1} at $i = 90^\circ$. The rotational frequency for a γ Doradus star is expected to be on the same order as the pulsation frequency and these values fall within this range.

The pulsation parameter tool can be used to get an indication of the horizontal-to-vertical pulsation amplitude parameter (κ) and whether the pulsation and rotation frequencies fall within the mode determination limits of FAMIAS. The κ value falls between the values 50-800 for frequencies $f_1 - f_2$, which is above 1.0 as expected for γ Doradus stars. These values then show the natural pulsational frequencies to lie between 0.2 d^{-1} and 0.7 d^{-1} . Taking the ratio f_{rot}/f_{co-rot} gives values in the range 1-5 for the determined frequencies and modes (all $m = 1$). FAMIAS has an operational range of $f_{rot}/f_{co-rot} \leq 0.5$, being designed to deal with p-mode pulsations with much larger vertical pulsation components. The very high values of κ for the g-mode pulsations in γ Doradus stars and the high rotation rate of this star mean we are operating beyond this limit. To obtain a reasonable mode identification the mass and radius were extended to non-physical values for a γ Doradus star to provide observable amplitudes of pulsation (see Table 8). However the mass and radius are solely used for the calculation of the ratio κ , and do not affect other aspects of the fit. Making these changes allowed us to consider pulsations with f_{rot}/f_{co-rot} values of 0.3-0.5 for the multi-frequency fit in Table 9.

Including more physics to more accurately describe the effects of rotation of g-modes in current pulsation models would ultimately solve such problems. Townsend (2003) investigated the effect of higher rotation on g-modes with high n and low l by increasing the Coriolis forces. It was seen that the identification of prograde modes (defined here as $m > 0$, in Townsend 2003 as $m < 0$), have smaller differences in the rotating scenarios than retrograde modes. Smaller values of m are also less affected. There is also a discussion of this in Wright et al. (2011) who estimate the true limits of the

Table 8. Stellar parameters used in the mode identification. Fixed values for T_{eff} , $[M/H]$ and $\log g$ were taken from Bruntt et al. (2008) and $v \sin i$ values from the ranges in Bruntt et al. (2008); De Cat et al. (2006); Dupret et al. (2005); Aerts et al. (2004); Eyser & Aerts (2000).

Parameter	Fixed Value	Min	Max	Step
Radius (solar units)		1	10	0.1
Mass (solar units)		0.5	50	0.01
Temperature (K)	7193			
Metallicity $[M/H]$	0.13			
$\log g$	4.18			
Inclination ($^\circ$)		0	90	1
$v \sin i$ (km s^{-1})		60	75	0.1

Table 9. Results of mode identification of all four frequencies individually after a least-squares fit is applied (lsf), and all four frequencies simultaneously (sim).

	Mode ID	χ^2	Inc. ($^\circ$)	Amp (km s^{-1})	Ph.
f_1 lsf	(1,1)	7.65	43.15	0.82	0.32
f_2 lsf	(1,1)	7.00	35.79	0.74	0.80
f_3 lsf	(1,1)	7.57	22.40	1.50	0.18
f_4 lsf	(1,1)	10.43	33.11	1.50	0.72
f_5 lsf	(1,1)	5.49	33.11	0.50	0.61
f_1 sim	(1,1)	16.59	29.67	2.06	0.31
f_2 sim	(1,1)			1.07	0.81
f_3 sim	(1,1)			2.90	0.18
f_4 sim	(1,1)			1.07	0.71
f_5 sim	(1,1)			2.17	0.60

$f_{\text{rot}}/f_{\text{co-rot}}$ ratio in FAMIAS for various m for a γ Doradus range frequency and found FAMIAS could identify modes up to $f_{\text{rot}}/f_{\text{co-rot}} = 1$ for a $m = 1$ mode. These results indicate that the mode identification is unlikely to be affected by the rotation of this star. We can be confident that using non-physical values for mass and radius affects only the observed amplitude of the pulsation and not the mode, itself.

A convincing mode identification of the frequencies $f_1 - f_5$ was obtained.

6 DISCUSSION

This study allowed a direct comparison between single-site and multi-site data. From this we can judge the usefulness of large single-site datasets. The findings show that although the addition of further sites increased the amplitudes of the frequencies, it also elevated the base noise level. Additionally it is clear from the window function spectra in Figure 2 that the 1-day aliasing pattern is reduced but not entirely eliminated. The above leads us to conclude that the addition of multi-site data is useful, but not required to extract frequencies from sufficiently large datasets. We must also require that the data from any one site have a sufficient number of observations to produce a balanced (well sampled in phase space) mean line profile in order to combine the cross-correlated line profiles with the highest precision.

The frequencies found in the PbP method were the most reliable and were consistent with all the other analysis methods. Past papers have analysed the photometric data from

HIPPARCOS and also some multi-coloured photometry. In Handler (1999), the author finds a frequencies of 2.18 d^{-1} and 1.2155 d^{-1} (f_{p4}). In this paper we found frequencies f_{p4} , f_{p5} and $(2x) f_{p8}$ in the HIPPARCOS photometry.

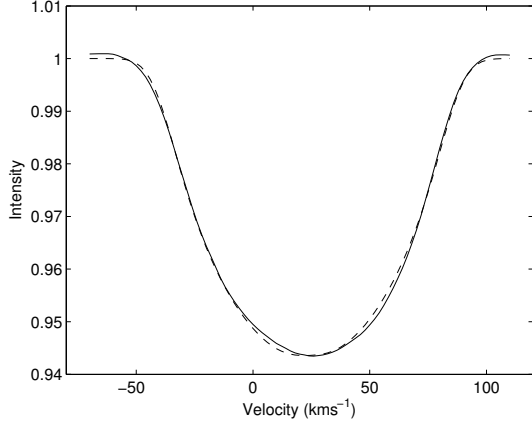
The multi-colour photometry was previously published by Aerts et al. (2004), who found frequencies equivalent to f_{p4} , f_{p1} and a 1-day alias of f_{p3} . In the same data we find f_{p4} , f_{p1} and f_{p5} . The mode identification showed the frequencies f_{p4} , f_{p1} and f_{p3} to best fit $l = 1$ modes, the same as found in this analysis. The same result was found by Dupret et al. (2005) who showed that the three frequencies from Aerts et al. (2004) are $l = 1$ modes when using time-dependent convection models.

Aerts et al. (2004) also describe the spectroscopic dataset taken with CORALIE that was also used in this analysis. The authors did not find any frequencies from the spectroscopic data alone (it is, as the authors note, too small a dataset for spectroscopic analysis). The imposition of the f_{p4} , f_{p1} frequencies found in their photometric analysis did provide some harmonic fits with low amplitudes.

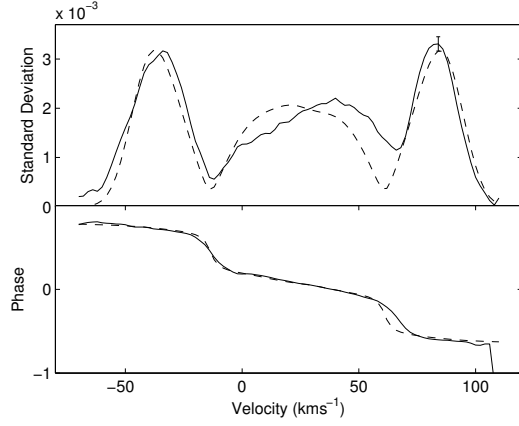
A study applying the frequency ratio method to the frequencies found in Aerts et al. (2004) was done by Moya et al. (2005), who found three models consistent with $l = 1$ modes. The models have a $T = 6760 \text{ K}$, $\log g = 3.88 - 4.12$ and stellar ages around $2 - 3 \text{ Myr}$.

Considering all the prior studies, all of the candidate frequencies we confirm (f_{p1} to f_{p5} and f_{p8}) are well supported. The mode identification is also partially confirmed by photometry. There is no suggestion of different frequencies observed in photometry and spectroscopy as there are from some γ Doradus stars (see Maisonneuve et al. 2011; Uytterhoeven et al. 2008).

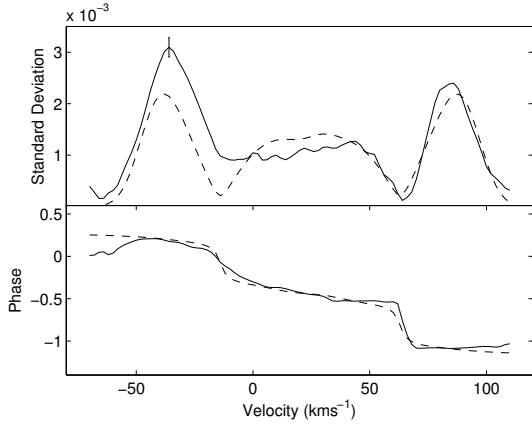
A prevalence of (1,1) modes in this star, and in γ Doradus stars in general, is beginning to emerge. This includes two modes in HD 135825 (Brunsden et al. 2012), two in γ Doradus (Balona et al. 1996; Dupret et al. 2005), one in HD 40745 (Maisonneuve et al. 2011), one in HR8799 (Wright et al. 2011), two in HD 189631 (Davie 2011) and two in HD 65526 (Greenwood 2012). This is possibly due to the large surface area covered in each segment of a (1,1) mode, meaning pulsations have larger amplitudes and large changes in amplitude across the stellar surface. This indicates an observational selection effect. Additionally Balona et al. (2011) discuss the prevalence of $m = \pm 1$ modes in a sample of γ Doradus candidates from *Kepler* photometry. These authors assume the dominant frequency to be the rotational frequency and they then show further frequencies to be close to this value. This constrains the light maxima to once per rotation cycle, requiring a $m = \pm 1$ mode. The occurrence of five of these such modes in this star suggests some physical linking between them. The identification of several (1,1) modes in this star led to an investigation into the period spacings of the six identified frequencies (Table 3). The asymptotics of oscillation theory (Tassoul 1980) predicts a characteristic period spacing for high-order g-modes of the same low degree (l) for sequential values of n . An investigation into the period spacings of the PbP identified frequencies shows that the spacing between $f_{p1}-f_{p2}$ and $f_{p1}-f_{p3}$ to be close (0.1266d and 0.1215d respectively). This suggests they could be subsequent values of n if we allow our frequencies to vary by $\pm 0.003 \text{ d}^{-1}$. The frequencies f_{p4} , f_{p5} and f_{p8} however do not fit with this spacing and addi-



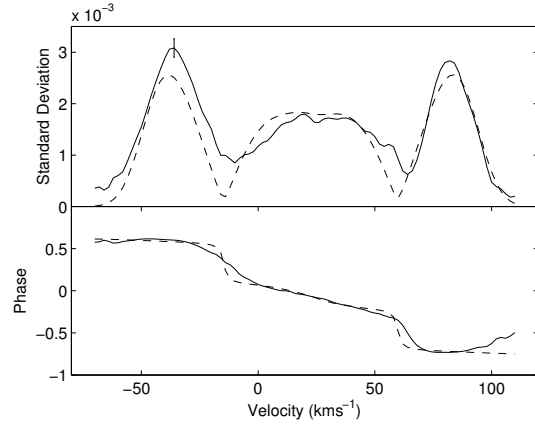
(a) Fit of the zero-point profile ($\chi^2 = 104$).



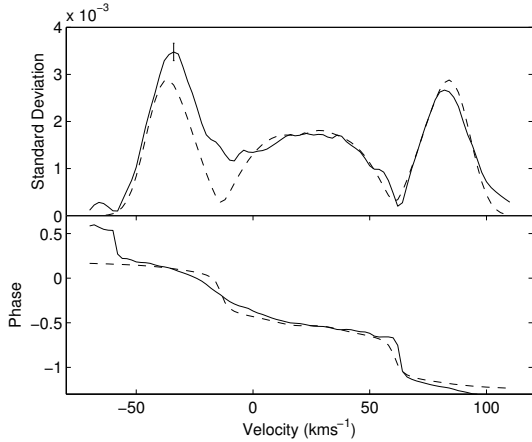
(b) Mode identification of $f_{p1} = 1.3959 \text{ d}^{-1}$ ($\chi^2 = 7.7$).



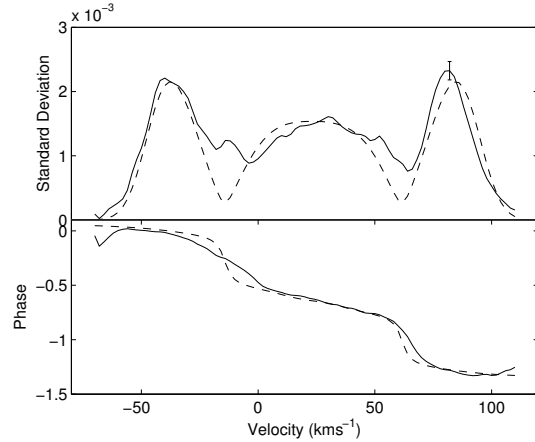
(c) Mode identification of $f_{p2} = 1.1863 \text{ d}^{-1}$ ($\chi^2 = 7.0$).



(d) Mode identification of $f_{p3} = 1.6812 \text{ d}^{-1}$ ($\chi^2 = 7.6$).



(e) Mode identification of $f_{p4} = 1.2157 \text{ d}^{-1}$ ($\chi^2 = 10.4$).

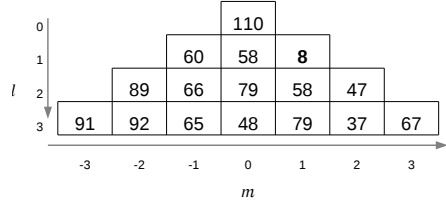


(f) Mode identification of $f_{p5} = 1.5596 \text{ d}^{-1}$ ($\chi^2 = 5.5$).

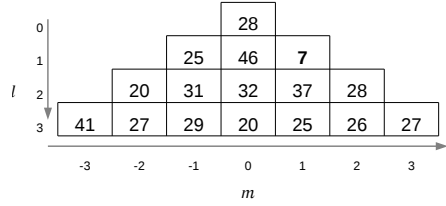
Figure 5. The fit (dashed) of the mode identification to the mean line profile, variation and phase (solid) of the five identified frequencies. All have been identified as (1,1) modes with the labelled χ^2 for the best fit. An indication of the maximum uncertainty is given on each plot.

tionally it may be that the close spacing of f_{p2} and f_{p4} is inconsistent with current theoretical models. The identification of the frequencies could be further improved by photometric studies to confirm this. Ultimately the sequencing of n -values could provide us with direct information about the stellar interior.

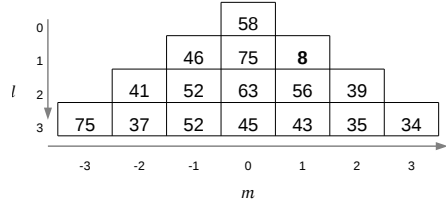
For the reasons above we propose this star as an excellent candidate with which to test asteroseismic models and potentially give us insight into the pulsational behaviour of γ Doradus stars.



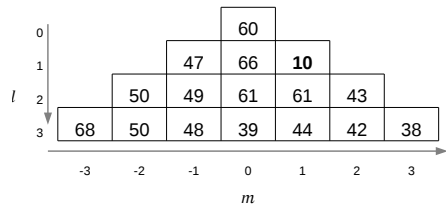
(a) χ^2 values for $l = 0 - 3$ for $f_{p1} = 1.3959\text{d}^{-1}$. Best fit value is for $(l, m) = (1, 1)$.



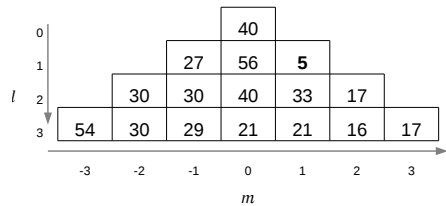
(b) χ^2 values for $l = 0 - 3$ for $f_{p2} = 1.1863\text{d}^{-1}$. Best fit value is for $(l, m) = (1, 1)$.



(c) χ^2 values for $l = 0 - 4$ for $f_{p3} = 1.6812\text{d}^{-1}$. Best fit value is for $(l, m) = (1, 1)$.



(d) χ^2 values for $l = 0 - 3$ for $f_{p4} = 1.2157\text{d}^{-1}$. Best fit value is for $(l, m) = (1, 1)$.



(e) χ^2 values for $l = 0 - 3$ for $f_{p5} = 1.5596\text{d}^{-1}$. Best fit value is for $(l, m) = (1, 1)$.

Figure 6. Lowest χ^2 values for each possible (l, m) combination for the final identified frequencies. The best fit χ^2 is identified in bold.

7 ACKNOWLEDGEMENTS

This work was supported by the Marsden Fund administered by the Royal Society of New Zealand.

The authors acknowledge the assistance of staff at Mt John University Observatory, a research station of the University of Canterbury.

We appreciate the time allocated at other facilities for multi-site campaigns, particularly McDonald Observatory and La Silla (European Southern Observatory).

Gratitude must be extended to the numerous observers who make acquisition of large datasets possible. We thank P. M. Kilmartin at MJUO and all the observers at La Silla and the HIPPARCOS team for their dedication to acquiring precise data.

This research has made use of the SIMBAD astronomical database operated at the CDS in Strasbourg, France.

Mode identification results obtained with the software package FAMIAS developed in the framework of the FP6 European Coordination action HELAS (<http://www.helas-eu.org/>).

We thank our reviewer Gerald Handler for his helpful comments that improved this paper.

8 SUPPORTING INFORMATION

Additional Supporting information may be found in the online version of this article:

Data file. The line profile data including Modified Julian Date, velocity (on a relative scale) and the intensity at each of the 120 velocity sampling points for each profile. Line 1 is the axis scale, lines 2-478 are MJUO observations, lines 479-526 are La Silla observations and lines 527-586 are McDonald observations.

References

- Aerts C., Cuypers J., De Cat P., Dupret M. A., De Ridder J., Eyer L., Scuflaire R., Waelkens C., 2004, A&A, 415, 1079
- Balona L. A., 1986, MNRAS, 219, 111
- Balona L. A., Böhm T., Foing B. H., Ghosh K. K., Janot-Pacheco E., Krisciunas K., Lagrange A.-M., Lawson W. A., James S. D., Baudrand J., Catala C., Dreux M., Felenbok P., Hearnshaw J. B., 1996, MNRAS, 281, 1315
- Balona L. A., Guzik J. A., Uytterhoeven K., Smith J. C., Tenenbaum P., Twicken J. D., 2011, MNRAS, 415, 3531
- Balona L. A., Stobie R. S., 1979, MNRAS, 189, 649
- Briquet M., Aerts C., 2003, A&A, 398, 687
- Brunsdon E., Pollard K. R., Cottrell P. L., Wright D. J., De Cat P., Kilmartin P. M., 2012, MNRAS, 422, 3535
- Bruntt H., De Cat P., Aerts C., 2008, A&A, 478, 487
- Chapellier E., Rodríguez E., Auvergne M., Uytterhoeven K., Mathias P., Bouabid M.-P., et al., 2011, A&A, 525, A23
- Cugier H., Dziembowski W. A., Pamyatnykh A. A., 1994, A&A, 291, 143
- Daszyńska-Daszkiewicz J., Dziembowski W. A., Pamyatnykh A. A., Goupil M.-J., 2002, A&A, 392, 151
- Davie M., 2011, Astr480 project, University of Canterbury

- De Cat P., Eyer L., Cuypers J., Aerts C., Vandenbussche B., Uytterhoeven K., Reyniers K., Kolenberg K., Groenewegen M., Raskin G., Maas T., Jankov S., 2006, *A&A*, 449, 281
- Dupret M.-A., Grigahcène A., Garrido R., De Ridder J., Scuflaire R., Gabriel M., 2005, *MNRAS*, 360, 1143
- Eyer L., Aerts C., 2000, *A&A*, 361, 201
- Greenwood A., 2012, Astr391 project, University of Canterbury
- Grigahcène A., Antoci V., Balona L., Catanzaro G., Daszyńska-Daszkiewicz J., Guzik J. A., Handler G., Houdek G., Kurtz D. W., Marconi M., Monteiro M. J. P. F. G., et al., 2010, *ApJ*, 713, L192
- Grigahcène A., Dupret M.-A., Sousa S. G., Monteiro M. J. P. F. G., Garrido R., Scuflaire R., Gabriel M., 2012, *MNRAS*, 422, L43
- Guzik J. A., Kaye A. B., Bradley P. A., Cox A. N., Neuforge C., 2000, *ApJ*, 542, L57
- Handler G., 1999, *MNRAS*, 309, L19
- Henry G. W., Fekel F. C., 2005, *AJ*, 129, 2026
- Henry G. W., Fekel F. C., Henry S. M., 2011, *AJ*, 142, 39
- Kallinger T., Reegen P., Weiss W. W., 2008, *A&A*, 481, 571
- Kaye A. B., 2007, *Communications in Asteroseismology*, 150, 91
- Kaye A. B., Handler G., Krisciunas K., Poretti E., Zerbi F. M., 1999, *PASP*, 111, 840
- Maisonnette F., Pollard K. R., Cottrell P. L., Wright D. J., De Cat P., Mantegazza L., Kilmartin P. M., Suárez J. C., Rainer M., Poretti E., 2011, *MNRAS*, 415, 2977
- Montgomery M. H., Odonoghue D., 1999, *Delta Scuti Star Newsletter*, 13, 28
- Moya A., Suárez J. C., Amado P. J., Martín-Ruiz S., Garrido R., 2005, *A&A*, 432, 189
- Perryman M. A. C., ESA eds, 1997, *The HIPPARCOS and TYCHO catalogues. Astrometric and photometric star catalogues derived from the ESA HIPPARCOS Space Astrometry Mission Vol. 1200 of ESA Special Publication*
- Pollard K. R., 2009, in J. A. Guzik & P. A. Bradley ed., *American Institute of Physics Conference Series Vol. 1170 of American Institute of Physics Conference Series, A Review Of γ Doradus Variables*. pp 455–466
- Reegen P., 2007, *A&A*, 467, 1353
- Tassoul M., 1980, *ApJS*, 43, 469
- Townsend R. H. D., 2003, *MNRAS*, 343, 125
- Uytterhoeven K., Mathias P., Poretti E., Rainer M., Martín-Ruiz S., Rodríguez E. and Amado P. J., Le Contel D., Jankov S., Niemczura E., Pollard K. R., Brunsden E., Paparó M., Costa V., et al., 2008, *A&A*, 489, 1213
- Uytterhoeven K., Moya A., Grigahcène A., Guzik J. A., Gutiérrez-Soto J., Smalley B., Handler G., Balona L. A., Niemczura E., Fox Machado L., Benatti S., Chapellier E., Tkachenko A., et al., 2011, *AAP*, 534, A125
- Watson R. D., 1988, *APSS*, 140, 255
- Wright D. J., 2008, PhD thesis, University of Canterbury
- Wright D. J., Chené A.-N., De Cat P., Marois C., Mathias P., Macintosh B., Isaacs J., Lehmann H., Hartmann M., 2011, *ApJL*, 728, L20
- Wright D. J., Pollard K. R., Cottrell P. L., 2007, *CoAst*, 150, 135
- Zima W., 2008, *CoAst*, 157, 387
- Zima W., 2009, *A&A*, 497, 827
- Zima W., Wright D., Bentley J., Cottrell P. L., Heiter U., Mathias P., Poretti E., Lehmann H., Montemayor T. J., Breger M., 2006, *A&A*, 455, 235